Title

Large-Area, Ultrathin Metal-Oxide Semiconductor Nanoribbon Arrays Fabricated by Chemical Lift-Off Lithography.

Journal

Nano letters, 18(9)

ISSN

1530-6984

Authors

Zhao, Chuanzhen
Xu, Xiaobin
Bae, Sang-Hoon
et al.

Publication Date

2018-09-01

DOI

10.1021/acs.nanolett.8b02054

Peer reviewed

HHS Public Access

Author manuscript

Nano Lett. Author manuscript; available in PMC 2019 April 15.

Published in final edited form as:

Nano Lett. 2018 September 12; 18(9): 5590–5595. doi:10.1021/acs.nanolett.8b02054.

Large-Area, Ultrathin Metal-Oxide Semiconductor Nanoribbon Arrays Fabricated by Chemical Lift-Off Lithography

Chuanzhen Zhao[†,§], **Xiaobin Xu**[†,§], **Sang-Hoon Bae**[†,□], **Qing Yang**[†,§], **Wenfei Liu**[†,§], **Jason N. Belling**[†,§], **Kevin M. Cheung**[†,§], **You Seung Rim**[†,□,¶], **Yang Yang**[†,□], **Anne M. Andrews**[*,†,§,▽], and **Paul S. Weiss**[*,†,§,□]

[†] California NanoSystems Institute, University of California, Los Angeles, Los Angeles, California 90095, United States

[§] Department of Chemistry and Biochemistry, University of California, Los Angeles, Los Angeles, California 90095, United States

[□] Department of Materials Science and Engineering, University of California, Los Angeles, Los Angeles, California 90095, United States

[▽] Department of Psychiatry and Biobehavioral Sciences, Semel Institute for Neuroscience and Human Behavior, and Hatos Center for Neuropharmacology, University of California, Los Angeles, Los Angeles, California 90095, United States

[¶] School of Intelligent Mechatronics Engineering, Sejong University, Seoul 05006, Republic of Korea

Abstract

Nanoribbon- and nanowire-based field-effect transistors (FETs) have attracted significant attention due to their high surface-to-volume ratios, which make them effective as chemical and biological sensors. However, conventional nanofabrication of these devices is challenging and costly posing a major barrier to widespread use. We report a high-throughput approach for producing arrays of ultrathin (~3 nm) In_2O_3 nanoribbon FETs at wafer scale. Uniform films of semiconducting In_2O_3 were prepared on Si/SiO_2 surfaces *via* a sol-gel process, prior to depositing Au/Ti metal layers. Commercially available HD-DVDs were employed as low-cost, large-area templates to prepare polymeric stamps for chemical lift-off lithography (CLL), which selectively removed molecules from self-assembled monolayers functionalizing the outermost Au surfaces. Nanoscale chemical patterns, consisting of one-dimensional lines (200 nm wide, 400 nm pitch) extending over centimeter length scales, were etched into the metal layers using the unpatterned monolayer regions as resists. Subsequent etch processes transferred the patterns into the underlying In_2O_3

[*]**Corresponding Authors** aandrews@mednet.ucla.edu, psw@cnsi.ucla.edu.

Author Contributions

The experiments were designed by CZ, AMA, and PSW. Data were collected by CZ, XX, SHB, QY, WL, JNB, and KMC, and were analyzed by CZ, XX, YSM, YY, AMA, and PSW. Figures were prepared by CZ and XX. The manuscript was written by CZ, XX, AMA, and PSW with assistance from all other authors.

Supporting Information.

Experimental details; Figure S1-S3; Fabrication process of HD DVD masters, DVD-masters, Si masters and *h*-PDMS stamps; Characterization of chemical patterns and stamps; Surface functionalization; Activation of PDMS stamps; Au, Ti, and In_2O_3 selective wet-etching processes; Surface roughness characterization of the In_2O_3; Photographs of fabricated devices and FETs measurements; Photograph of interdigitated electrodes.

films before removing the protective organic and metal coatings, revealing large-area nanoribbon arrays. We employed nanoribbons in semiconducting FET channels, achieving current on/off ratios over 10^7 and carrier mobilities up to 13.7 $cm^2 V^{-1} s^{-1}$. Nanofabricated structures, such as In_2O_3 nanoribbons and others, will be useful in nanoelectronics and biosensors. The technique demonstrated here will enable these applications and expand low-cost, large-area patterning strategies to enable a variety of materials and design geometries in nanoelectronics.

Table of Contents Graphic and Synopsis

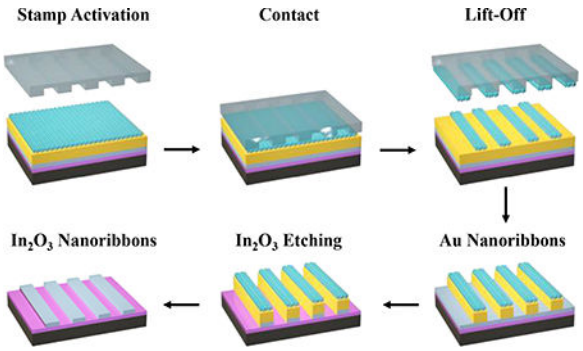

Keywords

soft lithography; chemical lift-off lithography; nanolithography; indium oxide; metal oxide semiconductors; field-effect transistor; nanoribbon; biosensor

One-dimensional (1D) nanomaterials, such as nanowires, nanotubes, and nanoribbons, possess large surface-to-volume ratios and tunable physical properties. These characteristics can be leveraged to achieve superior performance over bulk materials in a variety of applications, including electronics,[1–5] optics and photonics,[6–10] energy-storage and conversion devices,[11,12] biological and chemical sensors,[13–19] intracellular delivery of bioactive molecules,[20] and medical devices.[21,22] For example, Si nanowires (SiNWs) and carbon nanotubes (CNTs) have been employed as channel components in field-effect transistors (FETs) for highly effective sensing of proteins,[23,24] DNA,[25,26] viruses,[27] and neurotransmitters.[28] However, significant problems remain to be solved before 1D nanomaterials find widespread use.

Bottom-up techniques, such as chemical vapor deposition (CVD) and solution processes,[29–33] dominate 1D-nanomaterial fabrication. However, these strategies have poor control over the orientations of as-grown nanostructures, often on substrates other than the final devices. Bottom-up methods require additional steps to transfer nanostructures and then to control their positions and orientations in devices.[34,35] For example, SiNWs and CNTs, typically synthesized by CVD, require precise control over specific growth parameters to produce high-quality 1D nanomaterials suitable for electronic devices.[29,36] Moreover, nanowires synthesized by CVD are randomly orientated greatly increasing the complexity of device fabrication.[37] Performance is limited by poor control over the numbers of functional nanowires present in devices.[38,39]

Top-down approaches, including photolithography and electron-beam lithography (EBL), are widely used in the semiconductor industry to fabricate 1D nanomaterials. Top-down methods enable precise control over final shapes, sizes, positions, and orientations of the as-fabricated structures,[40,41] providing ready integration with devices and high reproducibility.[42,43] Nonetheless, top-down techniques suffer from substantial equipment and usage costs. Patterns produced *via* photolithography are limited by the resolution of the optical imaging system, often to micron-scale features. By contrast, EBL achieves nanometer-resolution patterning but at the expense of time-consuming serial writing processes. These drawbacks represent significant barriers for many users, hence the need for alternative high-throughput, economical nanoscale patterning strategies.

Recently, we reported a straightforward, high-fidelity nanopatterning technique called chemical lift-off lithography (CLL),[44–48] wherein oxygen plasma-activated polydimethylsiloxane (PDMS) stamps selectively remove portions of a self-assembled monolayer (SAM) in contacted areas without observable lateral diffusion at feature edges. The remaining SAM molecules in the non-contacted regions act as molecular resists during subsequent etching of the freshly exposed underlying substrate. We previously demonstrated that CLL can be used to simplify device fabrication, as well as to enable biomolecule patterning to investigate DNA hybridization and spin-selective electron transport.[49–53] High-fidelity chemical patterns with line widths as narrow as 40 ± 2 nm were achieved using CLL, with the possibility of features as narrow as 5 nm (corresponding to ~10 molecules).[46] As with other top-down patterning approaches, however, CLL relies on expensive nanofabricated masters to create PDMS stamps to produce nanoscale structures. Masters for CLL have been produced using low-throughput EBL methods, limiting impact.[47,48]

Many top-down nanofabrication processes, including CLL, have focused on patterning metals and group IV and III-V semiconductors (*e.g.*, Au and Si).[54] Metal oxides represent an increasingly important material class in numerous applications due to their electronic, mechanical, and optical properties.[45,55–57] To date, top-down approaches for fabricating metal-oxide nanomaterials are under developed compared to patterning methods for other types of materials, yet patterned semiconductors are of interest for applications including electronics, displays and lighting, ultra-sensitive biosensors, and wearable, flexible sensors.[58–60]

We report on the fabrication of large-area In_2O_3 nanoribbon arrays using CLL, but without using masters generated *via* EBL. We utilize metal oxide nanoribbons as semiconducting channels in FET architectures. Through this demonstration, we extend the range and applicability of CLL patterning to nanoscale features on semiconducting, metal oxides for functional electronic devices, achieving current on/off ratios of ~10^7 and a peak mobility of 13.7 $cm^2\ V^{-1}\ s^{-1}$, in a low-cost, high-throughput manner.

Most commonly used thin-film metal oxide deposition strategies rely on physical/chemical vapor deposition methods, such as pulsed-laser deposition,[61] sputtering,[62] and atomic-layer deposition,[63] requiring complex processes, extreme conditions (*e.g.*, high temperature, vacuum), and costly equipment. Recently, simple, scalable sol-gel-based processes have emerged as alternatives for preparing high quality semiconducting metal-oxide films.[64–67]

Here, thin films of In_2O_3 were prepared *via* a sol-gel process. Aqueous solutions (0.1 M) of $In(NO_3)_3$ were spin-coated onto SiO_2/Si substrates (100 nm, thermally grown SiO_2 dielectric on heavily doped, *p*-type Si substrates with resistivities of 1–5 mΩ·cm). Following deposition, substrates were heated to 100 °C for 5 min and annealed at 250 °C for 3 h. The thicknesses of the resulting In_2O_3 films were ~3 nm with typical surface roughnesses of ~0.06 nm determined *via* atomic force microscopy (AFM) (**Figure S1**).

Commercially available optical storage media, such as compact discs (CDs) and DVDs are patterned with sub-micron periodic gratings that can be used directly as economical templates for soft lithography. We employed HD-DVDs as masters for CLL PDMS stamps. The HD-DVDs have quasi-1D feature widths of ~200 nm, spaced at a pitch of 400 nm. As shown in **Figure 1a**, each HD-DVD is composed of a protection layer (I), a reflective layer (II), a recording layer (III), and a polycarbonate layer (IV) composed of embossed concentric rings that form the basis of the patterns used herein. Layer IV was exposed simply by removing layers I and II with a razor blade and dissolving layer III with ethanol (**Figure 1c**). Atomic force microscopy (AFM) confirmed the expected, grooved pattern on the surface of layer IV, as seen in **Figure 1e**. To replicate layer IV features precisely, hard PDMS (*h*-PDMS) was used as the stamp material due to its stiffness compared to regular (soft) Sylgard 184 PDMS.[68] Unpolymerized *h*-PDMS was spin-coated onto masters (2 cm × 2 cm, 40 s at 1000 rpm) and cured at 65 °C for 10 min to form thin and robust films. A layer of soft PDMS (~5 mm) was then applied and cured at 65 °C overnight to form a support for the pattern-containing *h*-PDMS film and to prevent cracking, prior to demolding stamps from masters. These stamps (**Figure 1d**) are reusable and can be employed for repeated, wafer-scale CLL patterning. Atomic-force micrographs of patterned PDMS surfaces (**Figure 1f**) confirmed precise replication of HD-DVD features with depths of ~60 nm.

The scheme used to fabricate In_2O_3 nanoribbons is illustrated in **Figure 2**. *Step 1:* layers of Ti (10 nm) and Au (30 nm) were deposited on previously prepared In_2O_3 films. The Au/Ti/In_2O_3/SiO_2/Si stacks were then incubated in 1 mM ethanolic solutions of 11-mercapto-1-undecanol ($HSCH_2(CH_2)_9CH_2OH$) to form SAMs terminated with –OH moieties, enabling CLL patterning. *Step 2:* an oxygen plasma was used to “activate” PDMS stamp surfaces, generating siloxyl groups (SiOH). Stamps were then brought into conformal contact with SAMs. Condensation reactions occur between the hydroxyl- (–OH) terminated SAMs and the SiOH groups of the activated *h*-PDMS, forming covalent linkages (Si–O–SAM). *Step 3:* Upon removal of the stamps, molecules within the contracted regions of the SAMs were selectively removed transferring the stamp pattern to the monolayer. Notably, in the lift-off process, monolayers of Au atoms are also removed as Au–S bonds (between SAM molecules and the underlying Au substrate atoms) are stronger than Au–Au bonds in the substrates.

Scanning electron microscopy of CLL-patterned SAMs (**Figure 3a**) confirmed the presence of 1D features (200 nm linewidths) over large areas, matching those on the stamps (**Figure 1f**). *Step 4:* Intact monolayers in the non-contacted regions acted as resists for successive etching by solutions of $Fe(NO_3)_3$ and thiourea (removing exposed Au) and EDTA disodium salt, NH_4OH, and H_2O_2 (removing Ti), thereby transferring the SAM patterns through the metal layers. The metal layers acted as etch masks protecting the underlying In_2O_3 films

from removal by glacial acetic acid. The resulting Au/Ti/In_2O_3 nanoribbons were investigated by AFM (**Figure 3b**) and found to have heights of ~45 nm, corresponding to the sum of the expected heights of the constituent layers above the surrounding Si/SiO_2 surfaces exposed by previous etch processes. *Step 5*: metal layers were completely removed to expose arrays of In_2O_3 nanoribbons extending over centimeter length scales (**Figure 3c**). The widths (~200 nm) and heights (~3 nm) of the metal oxide nanoribbons are the smallest, to our knowledge, fabricated *via* top-down approaches.

To demonstrate the versatility of CLL patterning for additional feature sizes, In_2O_3 nanoribbons of different linewidths (350 nm and 1500 nm) were fabricated using alternate master patterns (**Figure 3d and 3e**, respectively). The Au nanoribbons produced as an intermediate product of this process (*Step 4*) can also be used for a variety of applications, such as surface plasmon resonance biosensors. We note that In_2O_3 nanoribbon edges are rougher than those of similarly produced Au nanoribbons; this is a common phenomenon associated with isotropic etch processes, which can undercut regions below the protective masks.

Field-effect transistors have key advantages over optical or electrochemical platforms for biosensing applications, including low detection limits, real-time and label-free measurements, and simple integration with standard semiconductor-device processing.[45] To evaluate the performance of In_2O_3 nanoribbons in devices, we constructed FETs in a bottom-gate, top-contact configuration as shown in **Figure 4**. Gold electrodes were deposited atop arrays of as-prepared In_2O_3 nanoribbons *via* electron-beam evaporation through a shadow mask. As shown in **Figure S3**, interdigitated electrodes with widths of 1300 ɛm and lengths of 45 ɛm were used.

The spatially ordered arrangement of In_2O_3 nanoribbons on surfaces facilitated straightforward fabrication of FETs with consistent numbers of channels per device, controlled by the widths of the contact electrodes. Here, ~3000 200-nm-wide In_2O_3 nanoribbons were incorporated into each FET device. These FETs had high field-effect mobilities (μ_{sat}=10.0 ± 2.6 $cm^2\ V^{-1}\ s^{-1}$), averaged over 10 devices with a peak value of 13.7 $cm^2\ V^{-1}\ s^{-1}$ and a current on/off ratio $>10^7$. The performance of these devices exceeded those previously reported for 1D nanowire-based devices fabricated *via* bottom-up approaches. High-performance In_2O_3 nanoribbon FETs can be used in a variety of applications, such as ultrasensitive FET-based chemical, and biological sensors.

In summary, we report a high-throughput, large-scale strategy enabling fabrication of ultrathin, metal oxide nanoribbons that are readily integrated into devices. We leverage and extend the capabilities of CLL, in combination with selective etching processes, to pattern, successively, SAMs, metal films, and ultra-thin layers of In_2O_3 to create arrays of periodic, 1D nanostructures. Nanoribbons fabricated by this approach are uniform and continuous over centimeter scales. We demonstrate high performance FETs fabricated using In_2O_3 nanoribbons having carrier mobilities up to 13.7 $cm^2\ V^{-1}\ s^{-1}$ and on/off current ratios $>10^7$, making these nanoribbons promising materials for electronic devices, large-area displays, and sensors. By employing widely available low-cost HD-DVDs as nanostructured master patterns, in conjunction with CLL, a scalable and high-fidelity chemical patterning

technique that does not require sophisticated equipment and facilities, we lower barriers to nanostructure fabrication. The advances demonstrated here serve to extend large-area nanofabrication and to broadened application and user bases by providing alternative patterning strategies to photo- and electron-beam lithographies.

Supplementary Material

Refer to Web version on PubMed Central for supplementary material.

ACKNOWLEDGMENTS

This work was supported by National Science Foundation (CMMI-1636136) and the National Institute on Drug Abuse (DA045550). We acknowledge the facilities and thank the staff of the Nanoelectronics Research Facility (NRF), Electron Imaging Center, Nano & Pico Characterization Lab, and Integrated Systems Nanofabrication Cleanroom of the California NanoSystems Institute. The authors thank Dr. Jeffrey J. Schwartz for assistance in writing the manuscript.

REFERENCES

(1). Cui Y; Lieber CM Science 2001, 291, 851–853. [PubMed: 11157160]

(2). Xu X; Liu C; Kim K; Fan DL *Adv.* Funct. Mater. 2014, 24, 4843–4850.

(3). Memisevic E; Hellenbrand M; Lind E; Persson AR; Sant S; Schenk A; Svensson J; Wallenberg R; Wernersson LE Nano Lett. 2017, 17, 4373–4380. [PubMed: 28613894]

(4). Lee H; Manorotkul W; Lee J; Kwon J; Suh YD; Paeng D; Grigoropoulos CP; Han S; Hong S; Yeo J; Ko SH ACS Nano 2017, 11, 12311–12317. [PubMed: 29077403]

(5). Qiu C; Zhang Z; Xiao M; Yang Y; Zhong D; Peng LM Science 2017, 355, 271–276. [PubMed: 28104886]

(6). Huang MH; Mao S; Feick H; Yan H; Wu Y; Kind H; Weber E; Russo R; Yang P Science 2001, 292, 1897–1899. [PubMed: 11397941]

(7). Law M; Sirbuly DJ; Johnson JC; Goldberger J; Saykally RJ; Yang P Science 2004, 305, 1269–1273. [PubMed: 15333835]

(8). Xu X; Kim K; Fan D *Angew. Chem., Int.* Ed. 2015, 54, 2525–2529.

(9). Liu P; He X; Ren J; Liao Q; Yao J; Fu H ACS Nano 2017, 11, 5766–5773. [PubMed: 28521103]

(10). Xu X; Yang Q; Wattanatorn N; Zhao C; Chiang N; Jonas SJ; Weiss PS ACS Nano 2017, 11, 10384–10391. [PubMed: 28956898]

(11). Law M; Greene LE; Johnson JC; Saykally R; Yang P *Nat.* Mater. 2005, 4, 455–459. [PubMed: 15895100]

(12). Zhang L; Jia Y; Wang S; Li Z; Ji C; Wei J; Zhu H; Wang K; Wu D; Shi E; Fang Y; Cao A Nano Lett. 2010, 10, 3583–3589. [PubMed: 20715803]

(13). Kong J Science 2000, 287, 622–625. [PubMed: 10649989]

(14). Cui Y; Wei Q; Park H; Lieber CM Science 2001, 293, 1289–1292. [PubMed: 11509722]

(15). Li C; Zhang D; Liu X; Han S; Tang T; Han J; Zhou C *Appl.* Phys. Lett. 2003, 82, 1613–1615.

(16). Zhang D; Liu Z; Li C; Tang T; Liu X; Han S; Lei B; Zhou C Nano Lett. 2004, 4, 1919–1924.

(17). Cheng Y; Xiong P; Yun CS; Strouse GF; Zheng JP; Yang RS; Wang ZL Nano Lett. 2008, 8, 4179–4184. [PubMed: 19367840]

(18). Xu X; Li H; Hasan D; Ruoff RS; Wang AX; Fan DL *Adv. Funct.* Mater. 2013, 23, 4332–4338.

(19). Kim K; Xu X; Guo J; Fan DL *Nat.* Commun. 2014, 5, 3632. [PubMed: 24709694]

(20). Xu X; Hou S; Wattanatorn N; Wang F; Yang Q; Zhao C; Yu X; Tseng H-R; Jonas SJ; Weiss PS ACS Nano 2018, Article ASAP, DOI: 10.1021/acsnano.1028b00763.

(21). Kim J; Lee M; Shim HJ; Ghaffari R; Cho HR; Son D; Jung YH; Soh M; Choi C; Jung S; Chu K; Jeon D; Lee ST; Kim JH; Choi SH; Hyeon T; Kim DH Nat. Commun 2014, 5, 5747. [PubMed: 25490072]

(22). Liu R; Chen R; Elthakeb AT; Lee SH; Hinckley S; Khraiche ML; Scott J; Pre D; Hwang Y; Tanaka A; Ro YG; Matsushita AK; Dai X; Soci C; Biesmans S; James A; Nogan J; Jungjohann KL; Pete DV; Webb DB; Zou Y; Bang AG; Dayeh SA Nano Lett. 2017, 17, 2757–2764. [PubMed: 28384403]

(23). So HM; Won K; Kim YH; Kim BK; Ryu BH; Na PS; Kim H; Lee JO *J. Am. Chem.* Soc. 2005, 127, 11906–11907. [PubMed: 16117506]

(24). Stern E; Vacic A; Rajan NK; Criscione JM; Park J; Ilic BR; Mooney DJ; Reed MA; Fahmy TM *Nat.* Nanotechnol. 2010, 5, 138–142. [PubMed: 20010825]

(25). Hahm J. -i.; Lieber CM Nano Lett. 2004, 4, 51–54.

(26). Sorgenfrei S; Chiu CY; Gonzalez RL Jr.; Yu YJ; Kim P; Nuckolls C; Shepard KL *Nat.* Nanotechnol. 2011, 6, 126–132. [PubMed: 21258331]

(27). Patolsky F; Zheng G; Hayden O; Lakadamyali M; Zhuang X; Lieber CM *Proc. Natl. Acad.* Sci. U. S. A. 2004, 101, 14017–14022. [PubMed: 15365183]

(28). Li BR; Hsieh YJ; Chen YX; Chung YT; Pan CY; Chen YT *J.* Am. Chem. Soc. 2013, 135, 16034–16037. [PubMed: 24125072]

(29). Patolsky F; Zheng G; Lieber CM *Nat.* Protoc. 2006, 1, 1711–1724. [PubMed: 17487154]

(30). Wang ZL Science 2006, 312, 242–246. [PubMed: 16614215]

(31). Liu C; Xu X; Rettie AJE; Mullins CB; Fan DL J. Mater. Chem. A 2013, 1, 8111.

(32). Gao N; Zhou W; Jiang X; Hong G; Fu TM; Lieber CM Nano Lett. 2015, 15, 2143–2148. [PubMed: 25664395]

(33). Constantinou M; Rigas GP; Castro FA; Stolojan V; Hoettges KF; Hughes MP; Adkins E; Korgel BA; Shkunov M ACS Nano 2016, 10, 4384–4394. [PubMed: 27002685]

(34). Xu F; Durham JW; Wiley BJ; Zhu Y ACS Nano 2011, 5, 1556–1563. [PubMed: 21288046]

(35). Yao J; Yan H; Lieber CM *Nat.* Nanotechnol. 2013, 8, 329–335. [PubMed: 23603986]

(36). Alam SB; Panciera F; Hansen O; Molhave K; Ross FM Nano Lett. 2015, 15, 6535–6541. [PubMed: 26367351]

(37). Ishikawa FN; Curreli M; Chang HK; Chen PC; Zhang R; Cote RJ; Thompson ME; Zhou C ACS Nano 2009, 3, 3969–3976. [PubMed: 19921812]

(38). Li J; Zhang Y; To S; You L; Sun Y ACS Nano 2011, 5, 6661–6668. [PubMed: 21815637]

(39). Lee BY; Sung MG; Lee J; Baik KY; Kwon YK; Lee MS; Hong S ACS Nano 2011, 5, 4373–4379. [PubMed: 21615164]

(40). Stern E; Klemic JF; Routenberg DA; Wyrembak PN; Turner-Evans DB; Hamilton AD; LaVan DA; Fahmy TM; Reed MA Nature 2007, 445, 519–522. [PubMed: 17268465]

(41). Knopfmacher O; Tarasov A; Fu W; Wipf M; Niesen B; Calame M; Schonenberger C Nano Lett. 2010, 10, 2268–2274. [PubMed: 20499926]

(42). Tong HD; Chen S; van der Wiel WG; Carlen ET; van den Berg A Nano Lett. 2009, 9, 1015–1022. [PubMed: 19199755]

(43). Hwang SW; Lee CH; Cheng H; Jeong JW; Kang SK; Kim JH; Shin J; Yang J; Liu Z; Ameer GA; Huang Y; Rogers JA Nano Lett. 2015, 15, 2801–2808. [PubMed: 25706246]

(44). Liao WS; Cheunkar S; Cao HH; Bednar HR; Weiss PS; Andrews AM Science 2012, 337, 1517–1521. [PubMed: 22997333]

(45). Kim J; Rim YS; Chen H; Cao HH; Nakatsuka N; Hinton HL; Zhao C; Andrews AM; Yang Y; Weiss PS ACS Nano 2015, 9, 4572–4582. [PubMed: 25798751]

(46). Andrews AM; Liao WS; Weiss PS Acc. Chem. Res. 2016, 49, 1449–1457. [PubMed: 27064348]

(47). Xu X; Yang Q; Cheung KM; Zhao C; Wattanatorn N; Belling JN; Abendroth JM; Slaughter LS; Mirkin CA; Andrews AM; Weiss PS Nano Lett. 2017, 17, 3302–3311. [PubMed: 28409640]

(48). Zhao C; Xu X; Yang Q; Man T; Jonas SJ; Schwartz JJ; Andrews AM; Weiss PS Nano Lett. 2017, 17, 5035–5042. [PubMed: 28737930]

(49). Cao HH; Nakatsuka N; Serino AC; Liao WS; Cheunkar S; Yang H; Weiss PS; Andrews AM ACS Nano 2015, 9, 11439–11454. [PubMed: 26426585]

(50). Abendroth JM; Nakatsuka N; Ye M; Kim D; Fullerton EE; Andrews AM; Weiss PS ACS Nano 2017, 11, 7516–7526. [PubMed: 28672111]

(51). Cao HH; Nakatsuka N; Liao W-S; Serino AC; Cheunkar S; Yang H; Weiss PS; Andrews AM Chem. Mater. 2017, 29, 6829–6839.

(52). Chen CY; Wang CM; Chen PS; Liao WS Chem. Comm 2018.

(53). Chen CY; Wang CM; Chen PS; Liao WS Nanoscale 2018, 10, 3191–3197. [PubMed: 29372203]

(54). Ko H; Takei K; Kapadia R; Chuang S; Fang H; Leu PW; Ganapathi K; Plis E; Kim HS; Chen SY; Madsen M; Ford AC; Chueh YL; Krishna S; Salahuddin S; Javey A Nature 2010, 468, 286–289. [PubMed: 21068839]

(55). Rim YS; Bae SH; Chen H; Yang JL; Kim J; Andrews AM; Weiss PS; Yang Y; Tseng HR ACS Nano 2015, 9, 12174–12181. [PubMed: 26498319]

(56). Chen H; Rim YS; Wang IC; Li C; Zhu B; Sun M; Goorsky MS; He X; Yang Y ACS Nano 2017, 11, 4710–4718. [PubMed: 28430412]

(57). Rim YS; Chen H; Zhu B; Bae S-H; Zhu S; Li PJ; Wang IC; Yang Y *Adv.* Mater. Inter. 2017, 4, 1700020.

(58). Aroonyadet N; Wang X; Song Y; Chen H; Cote RJ; Thompson ME; Datar RH; Zhou C Nano Lett. 2015, 15, 1943–1951. [PubMed: 25636984]

(59). Liu Q; Aroonyadet N; Song Y; Wang X; Cao X; Liu Y; Cong S; Wu F; Thompson ME; Zhou C ACS Nano 2016, 10, 10117–10125. [PubMed: 27934084]

(60). Liu Q; Liu Y; Wu F; Cao X; Li Z; Alharbi M; Abbas AN; Amer MR; Zhou C ACS Nano 2018, 12, 1170–1178. [PubMed: 29338249]

(61). Nomura K; Ohta H; Takagi A; Kamiya T; Hirano M; Hosono H Nature 2004, 432, 488–492. [PubMed: 15565150]

(62). Martins RFP; Ahnood A; Correia N; Pereira LMNP; Barros R; Barquinha PMCB; Costa R; Ferreira IMM; Nathan A; Fortunato EE M. C. *Adv.* Funct. Mater. 2013, 23, 2153–2161.

(63). Lin YY; Hsu CC; Tseng MH; Shyue JJ; Tsai FY *ACS Appl.* Mater. Inter. 2015, 7, 22610–22617.

(64). Kim HS; Byrne PD; Facchetti A; Marks TJ *J.* Am. Chem. Soc. 2008, 130, 12580–12581. [PubMed: 18759390]

(65). Banger KK; Yamashita Y; Mori K; Peterson RL; Leedham T; Rickard J; Sirringhaus H Nat. Mater 2011, 10, 45–50. [PubMed: 21151167]

(66). Hwan Hwang Y; Seo J-S; Moon Yun J; Park H; Yang S; Ko Park S-H; Bae B-S NPG Asia Mater. 2013, 5, e45.

(67). Rim YS; Chen H; Song T-B; Bae S-H; Yang Y Chem. Mater 2015, 27, 5808–5812.

(68). Qin D; Xia Y; Whitesides GM *Nat.* Protoc. 2010, 5, 491–502. [PubMed: 20203666]

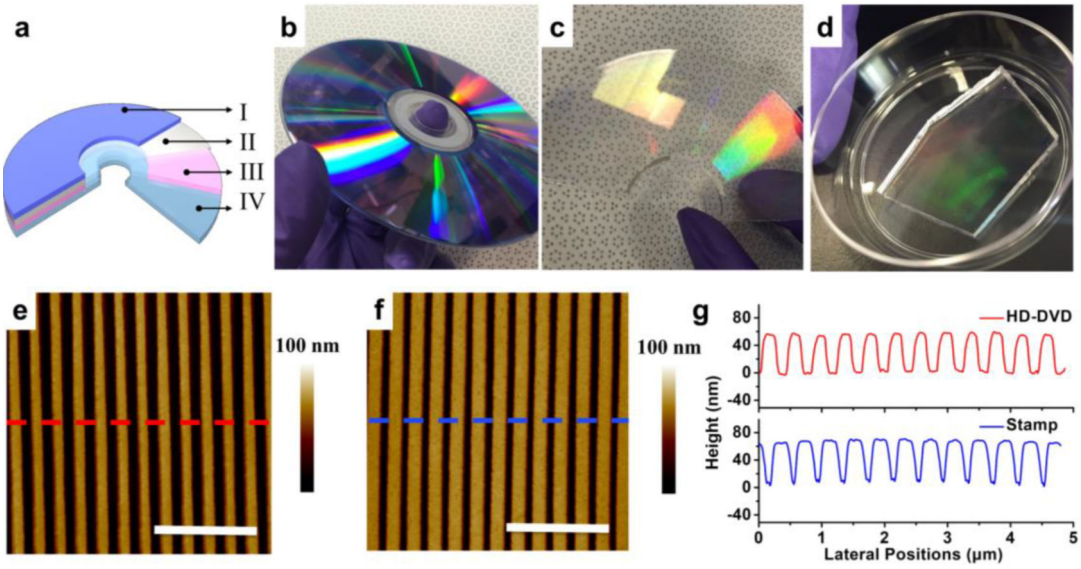

Figure 1.

(a) Schematic architecture of a high-definition digital-versatile disc (HD-DVD): Layer I, polycarbonate protective layer; Layer II, mirror-like metal film; Layer III, data recording film; Layer IV, polycarbonate layer containing concentric rings with typical widths of 250 nm and periodicities of 400 nm. (b-d) Photographs of an HD-DVD, an HD-DVD master (Layer IV), and a patterned polydimethylsiloxane (PDMS) stamp, respectively. Atomic force micrographs of a representative HD-DVD master (e) and a patterned PDMS stamp (f). Scale bars are 2 ɛm. (g) Topographic profiles across the corrugated features in (e) and (f).

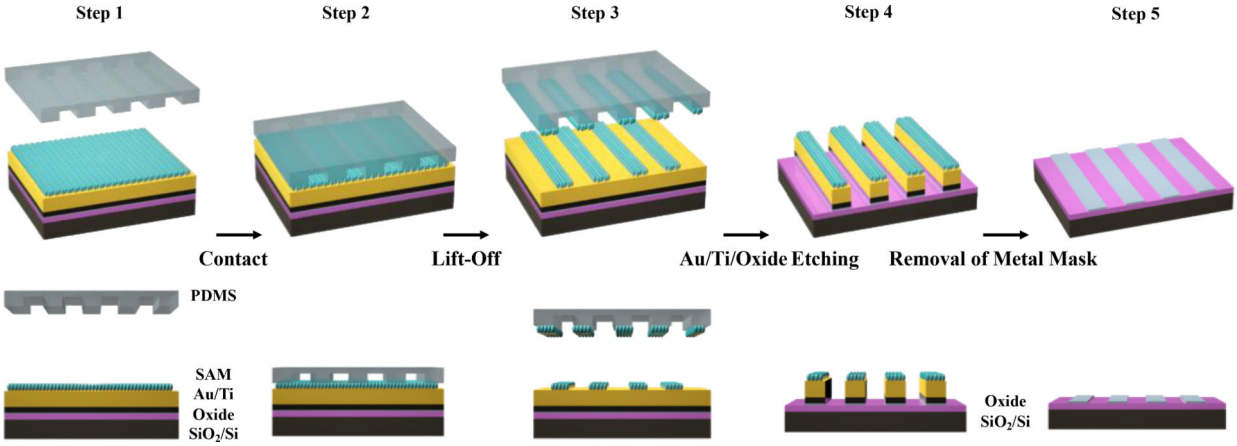

Figure 2.

Fabrication scheme of In_2O_3 nanoribbons. Step 1: a thin film of 3-nm In_2O_3 was deposited on a SiO_2/Si substrate *via* a sol-gel process followed by Au (30 nm)/Ti (10 nm) deposition and functionalization with a self-assembled monolayer (SAM). Step 2: a polydimethylsiloxane (PDMS) stamp, activated by an oxygen plasma, was brought into conformal contact with the substrate. Step 3: Upon lifting the stamp from the surface, SAM molecules in the contacted areas were removed, transferring the pattern (periodic lines and spaces) into the SAM. Step 4: Successive selective etch processes removed Au/Ti and In_2O_3 layers from unprotected regions on the surface. Step 5: Remaining SAM, Au, and Ti were removed to produce In_2O_3 nanoribbon arrays.

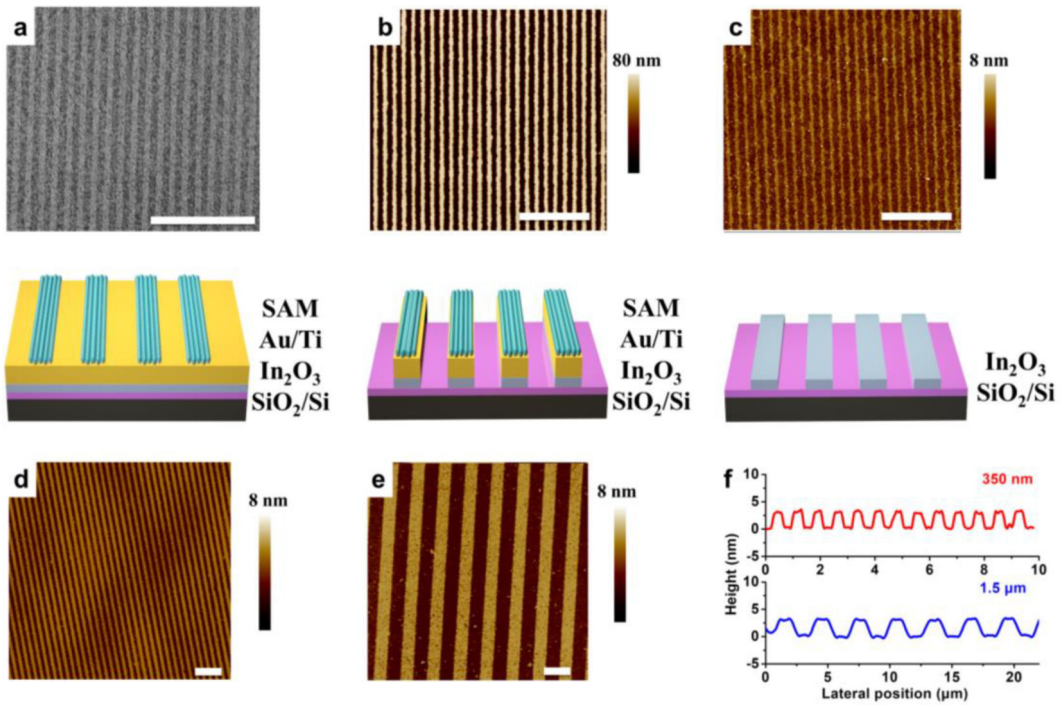

Figure 3.

(a) Scanning electron microscope image (top) and schematic (bottom) of a self-assemble monolayer (SAM) patterned *via* chemical lift-off lithography. (b, c) Topographic images measured using atomic force microscopy (AFM), top, and schematic illustrations, bottom, of SAM/Au/Ti/In_2O_3 and bare In_2O_3 nanoribbons, respectively, with line widths of ~200 nm. Atomic force topographs of In_2O_3 nanoribbons with line widths of (d) 350 nm and (e) 1.5 ɛm. Thicknesses of each set of In_2O_3 nanoribbons (c-e) were measured to be ~3 nm by AFM. (f) Height profiles of 500 nm wide In_2O_3 nanoribbons (top) and 1.5 ɛm wide nanoribbons (bottom). Scale bars in all images represent distances of 3 ɛm.

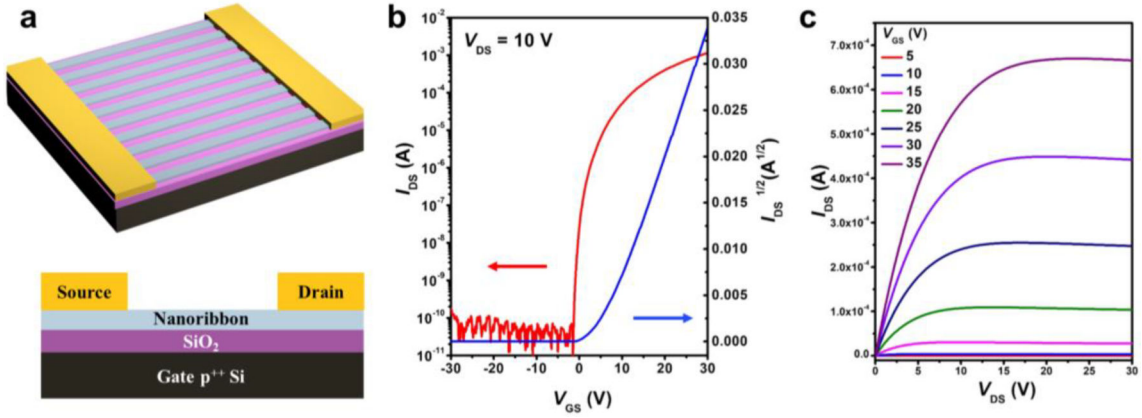

Figure 4.

(a) Schematic illustrations of an In_2O_3 field-effect transistor (FET) in a bottom-gate-top-contact configuration. Gate: Si (p^{++}); Source/Drain: Au; semiconducting channel: In_2O_3 nanoribbons. The widths and lengths of the inter-digital electrodes are 1300 and 45 ɛm, respectively. The widths and pitches of the nanoribbons are 200 and 400 nm, respectively. (b) Transfer and (c) output characteristics of an ultrathin In_2O_3 nanoribbon FET, showing the measured current between the drain and source (I_{DS}) in response to varying gate to source voltages (V_{GS}) and source to drain (V_{DS}) potentials, relative to the source. Devices displayed *n*-type pinch-off behavior with carrier motilities of 10.0 ± 2.6 $cm^2\ V^{-1}\ s^{-1}$, averaged over 10 devices with a peak value of 13.7 $cm^2\ V^{-1}\ s^{-1}$, and a current on/off ratio $>10^7$.